Refractive Laser Beam Measuring Diffusion Coefficient of Concentrated Battery Electrolytes

Katherine Betts¹, K Y Heenkenda¹, Bryan Jacome, Sohyo Kim, Michael Tovar, Zhange Feng*

Department of Chemistry and Biochemistry

University of Nevada, Las Vegas

4505 S Maryland Pkwy, Las Vegas, NV 89154, USA

Abstract

A thorough understanding of electrolyte transport properties is crucial in the development of alternative battery technology. As a key parameter, the diffusion coefficient offers important insights into the behavior of electrolytes, especially for fast charge of high-energy batteries. Existing methods of measurement are often limited by redox species or offer questionable accuracy due to side reactions and/or disruption of the diffusion profile. This work provides a novel optical method for measuring diffusion coefficients of liquid-phase concentrated battery electrolytes without electrochemical reactions. The method relies on the deflection of a refractive laser beam passing through an electrolyte of a minor concentration gradient in a triangular diffusion column. The diffusion coefficient, *D*, for a range of zinc sulfate electrolytes was successfully extracted by correlating the position of the laser beam to its concentration. Several other physicochemical properties of the same electrolytes are studied to correlate to the concentration-dependent diffusion coefficients, including viscosity, conductivity, and microstructure analysis based on vibrational spectroscopy (Infrared and Raman). Also included is the future application of the triangular column for *in situ* electrochemical measurements.

* Correspond author: Zhange Feng

Email: zhange.feng@unlv.edu

Phone: 1-702-895-5729

¹ these authors contributed equally to the work

Introduction

The fast-growing deployment of electric vehicles and solar panels has significantly increased the demand for improved battery performance regarding safety, energy density, and cost. 1,2 One fundamental aspect of battery innovation is the search for new battery electrolytes with improved physiochemical properties, e.g., chemical/electrochemical stability, non-flammability, and transport properties. Specifically, improving the transport properties of battery electrolytes has been of intense interest to battery researchers, since the transport of concentrated electrolytes in the porous electrodes/separator is recognized as one of the limiting steps for the fast-charge of secondary batteries. 3,4 Therefore, reliable methods for the measurement of transport properties are essential when developing novel battery electrolytes.

There are three transport properties associated with binary electrolytes: diffusion coefficient, conductivity, and cationic transference number, as defined by Newman.⁵ The diffusion coefficient, a proportionality constant describing the relationship between flux and chemical potential gradient, plays a key role in understanding the rate performance of rechargeable batteries. Small diffusion coefficients lead to large concentration gradients, causing sluggish ion transportation and side reactions, ultimately leading to battery failure.⁶ The diffusion coefficient is specific to each electrolyte system since it is a function of ion size, viscosity, and temperature. Thus, it is commonplace for those developing new battery electrolytes to measure the required coefficient as the indicator for the performance of battery electrolyte.

Several methods were developed in the past to measure diffusion coefficients of battery electrolytes, such as Pulse Field Gradient Nuclear Magnetic Resonance (PFG-NMR), electrochemical methods, and optical methods. While some measurements are based on the diluted

solution theory, the concentrated solution theory (Onsager-Stefan-Maxwell theory) is more accurate since interactions among all species are considered, including solvent, cation, and anion.⁷

PFG-NMR considers the relationship between electromagnetic phenomena and thermodynamic behaviors and measures the self-diffusion of NMR active nuclei, e.g., Li, F, and H.⁸ A sequence of radio-frequency pulses and associated phase changes are tracked during the diffusion process and observed by increases in the amplitude of echo signals. ^{9,10} Another emerging powerful technique characterizing transport properties of battery electrolyte is electrophoretic NMR (eNMR), where the theoretical framework for both diluted and concentrated electrolyte are validated. ¹¹ Although NMR techniques have proven successful, they are applicable to limited electrolytes, specifically, they fail to measure NMR inactive nuclei, like Zn²⁺. Also, such microscopic methods can struggle with macroscopic sample motion, leading to inflation of diffusion rate. ¹²

Electrochemical methods are the most popular technique to characterize the transport properties of battery electrolytes. Newman et al. developed the theory of restricted diffusion in binary solutions and successfully applied it to a series of polymer electrolytes. ¹³ The open circuit potential of a symmetric cell made of lithium electrodes and polymer film was recorded after the initial polarization, and the diffusion coefficient could be extracted from the correlation of OCP vs. time. This method was also extended to liquid electrolytes in electrochemical cells. Other electrochemical techniques include cyclic voltammetry, chronoamperometry techniques, and diaphragm cells, although the theoretical basis for these methods is mostly Fick's law, the Einstein equation and Onsager-Fouss, instead of concentrated solution theory. ^{14,15,16} Nevertheless, electrochemical techniques are often limited by the formal potentials of the redox species involved, side reactions, and passivation of the electrode, especially for nonaqueous electrolytes.

The optical method to measure the diffusion coefficient has drawn much attention recently due to the high sensitivity and accuracy in the absence of electrochemical reactions as well as the development of more advanced spectroscopic techniques. The work can be traced back to the 19th century when Gouy measured Raleigh interference patterns in a diffusing column to calculate the diffusion coefficient.¹⁷ Almost a century later, Newman and Chapman reported their Rayleigh technique based on the OSM theory, although ultimately these techniques are limited by spatial image resolution. Stewart et al. reported the use of UV-vis absorption to measure diffusion coefficients in LiPF₆ electrolytic solutions, and the diffusion coefficient is also extracted from the OSM theory.⁶ Developments in optical methods have continued to depend on image-based measurements. Nishikawa et al. developed a technique using diffraction Moiré patterns at the interface between diffusion couples. 18 Li et al created an 'asymmetric liquid-core cylindrical lens' which creates measurable dispersion images to quantify diffusion.¹⁹ Diffusion coefficients were also measured by Raman spectroscopy. Chen et al demonstrated a custom microfluidic gradient generator to observe ZnSO₄ solutions pumped into linear channels.²⁰ The intensity of the v₁ sulfate Raman peak was calibrated and used to record changes in concentration during diffusion. diffusion coefficient Similarly, Fawdon al measured of Lithium et the bis(trifluoromethanesulfonyl)imide (LiFSI) electrolytes by calibrating the FSI bending peak in Raman spectrum. The operando scanning Raman microspectroscopy took place within an electrochemical cell, allowing for tandem measurement of the diffusion coefficient and transference number.²¹ Despite the significant progress with optical spectroscopic techniques, limitations in battery electrolyte characterization still exist: Raman spectroscopy only applies to electrolytes with Raman active features (also applies to UV-vis), and uncertainties could evolve

during complicated procedures to extract diffusion coefficients, such as deconvolution of Raman peaks.

Herein, we developed a universal optical method using a refractive beam passing through the concentrated electrolyte filled in a triangular diffusion column (Figures 1a and 1b). The novel method measures the deflection of a refracted laser beam using a photodiode-based position detector. The linear relationship between concentration and laser position allows observation of restricted diffusion in real time. Although demonstrated with a series of ZnSO₄ electrolytes, the unique method is universal to all transparent liquid electrolytes and is not limited by concentration. It offers improved accuracy due to the absence of adverse side reactions and highly sensitive position detector. To demonstrate the correlation between the macroscopic properties and microstructures of battery electrolytes, we further conducted measurements of refractive index, conductivity, viscosity, infrared spectroscopy, and Raman spectroscopy with the same electrolyte. Also included in the investigation, was an initial test on the *in situ* electrochemical triangular cell as shown in Figure 1c.

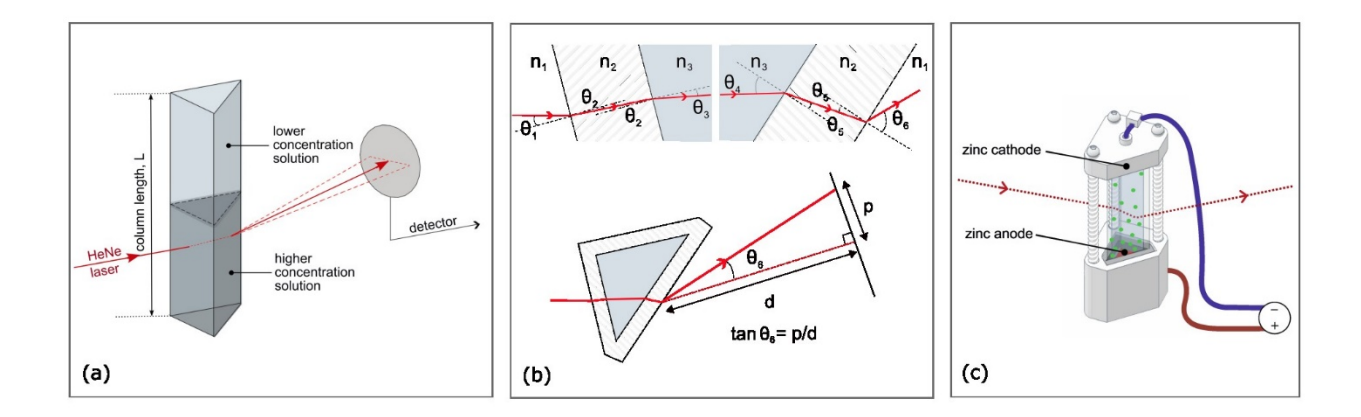


Figure 1: Schematics showing incidental and refracted beam passing through a triangular restricted diffusion column. (a) 3-dimensional optics schematic showing layering of solutions in

column length, L. (b) 2-dimensional optics demonstrating Snell's law calculations for theoretical modeling of laser deflection. (c) *in situ* triangular working cell.

Theoretical Aspects

When considering diffusion, it is best practice to start with Fick's law, which is the basis for the measurement of diffusion coefficients. Fick's second law describes the one-dimensional concentration gradient across a vertical diffusion column:

$$\frac{\partial c}{\partial t} = D \frac{\partial^2 c}{\partial y^2}$$
 [1]

According to Equation 1, if two solutions of different concentrations are layered on top of each other, the concentration on either side of the boundary condition changes with dependence on the rate of change in the concentration gradient. This 'free' diffusion becomes more complex when concentration changes reach the upper and lower boundaries of the column. At this point, we consider 'restricted diffusion' which intuitively leads to a ceasing of diffusion as the column reaches a homogeneous state. When considering the transport properties of battery electrolytes, we must model restricted diffusion as well as a multicomponent concentrated system. First, we look at the multicomponent diffusion equation proposed by Stefan-Maxwell, applied to solutions by Onsager²², and revisited by Newman's concentrated electrolyte theory:²³

$$c_{i} \nabla \mu_{i} = RT \sum_{j} \frac{c_{i} c_{j}}{c_{T} \mathfrak{D}_{ij}} (v_{j} - v_{i})$$
[2]

where ${}^{c}{}_{i}\nabla \mu_{i}$ is the thermodynamic driving force. The thermodynamic diffusion coefficient, \mathfrak{D}_{ij} , is unique to the specific concentration couple in the solution. In practice, it is common to measure the differential diffusion coefficient, D, which is related to \mathfrak{D}_{ij} by:

$$D = \mathfrak{D} \frac{c_T}{c_0} \left(1 + \frac{d \ln \gamma_{+-}}{d \ln m} \right)$$
 [3]

where γ_{+-} is the mean molal activity coefficient and m is molality.⁵ Harned and French's development of Onsager's work on diffusion resulted in a mathematical description of restricted diffusion as a concentration gradient Fourier series:¹³

$$c_t = c + \sum_{n=0}^{\infty} \left[A_n exp\left(\frac{-n^2 \pi^2 Dt}{L^2}\right) \cos\left(\frac{n\pi y}{L}\right) \right]$$
 [4]

where c_t represents the concentration at time, t, and c is the theoretical final concentration after diffusion is complete. L is the height of the restricted diffusion column; y is the distance from the bottom of the cell to the point of interest, and A_n is the activity coefficient of the electrolyte ions. Over long periods of time, the expanded Fourier Series can be simplified to the first term, because the series converges rapidly with time:

$$\frac{\ln(c_t - c)}{t} = -\frac{\pi^2 D}{L^2}$$
 [5]

By plotting $ln(c_t - c)$ against time, the slope of the linear stage of diffusion can be used to directly calculate the diffusion coefficient.

The novel method relies on the measurement of the time-resolved concentration profile by the deflection of the laser beam through the electrolyte in a triangular diffusion column. When light passes through the electrolyte, the deflection of the incident beam is dependent on the refractive index of the solution at that point, which is also a function of electrolyte concentration (Figure 1b). Therefore the position of the laser beam could be translated into the concentration of the electrolyte in the course of diffusion and the diffusion coefficient is calculated using Equation 5. The measured coefficient is specific to the electrolyte species and temperature of the solution.²⁴

Experimental

Chemicals: Zinc sulfate heptahydrate (assay 100.2%, J.T. Baker) and Millipore water (Barnstead, 18.2 M Ω -cm) were used to prepare a range of solutions from 0.10 mol/kg to 2.60 mol/kg

concentration. All solutions were prepared using molality (mol/kg) and later converted to molarity (c in mol/L) using a density calibration.

Diffusion measurements: A schematic diagram of the experimental setup is shown in Figure 1a. A polarized HeNe laser (MKS, model N-STP-912, 1 mW, 0.54 mm beam diameter) was arranged with a 1.0 optical density reflective neutral density filter (THORLABS) and a silicon photodiode-based lateral position detector (PDP90A, THORLABS) on an optical table. The detector has a specified resolution of 0.75μm and the sensitivity was optimized by positioning the detector. The laser was passed through a right-angled triangular quartz precision cell (15x11x11mm cross-section, 31mm length) at ~10mm from the base of the cell, rotated at ~3° anti-clockwise to the normal, and the cuvette was sealed with a PTFE plug. LabScribe software with a data accumulation card (iWorx) recorded the deflected position of the refractive beam.

For each reported concentration (final concentration at end of diffusion, c), a deflection calibration curve was produced to convert accumulated data for use with Equation 5. For each calibration, three trials at five concentrations in the range of the test were recorded for position. The diffusion measurements were made by layering two solutions of differing concentration (higher concentration at the base of the cell, lower concentration above), and recording the deflected position at a fixed height in the diffusion column. The upper solution was layered with the use of 3/64" heat shrink tubing, molded with an L-shaped end to slowly add the solution using a lmL syringe to avoid surface disturbance. The horizontal boundary between layers of differing density/concentration could be visibly deciphered by the eye. The experimental setup was enclosed and insulated to limit variations in external environmental conditions. The temperature of the electrolyte was kept constant at 22.4°C ± 0.2 °C using a copper refrigeration coil and circulation chiller with digital temperature control (VWR). Two 48-hour trials were run for each reported

coefficient to report an averaged value. Data points were collected every minute and smoothed to produce a concentration profile descriptive of the 48-hour diffusion. All final data was processed using Origin Pro 2023 software.

Characterization of physical properties: ZnSO₄ electrolytes were analyzed using an Abbe refractometer (Fisherbrand) for the refractive index and an Orian Star A212 conductivity meter (Thermo Scientific) for conductivity. A QCM-I Mini instrument and a standard flow cell from Gamry were used to determine the viscosity of ZnSO₄ electrolyte. Varying sample concentrations between 0.15mol/kg to 2.5mol/kg were tested to correspond with the reported diffusion coefficients. The flow cell was loaded with a 14 mm 5MHz quartz crystal sensor with gold electrode and set to 22°C. For the static flow-cell measurements, a syringe loaded with the analyte was manually pumped through the cell until the cell was filled with the desired electrolyte. The change in resonant frequency, Δf_n , of the nth overtone of the quartz crystal, was measured using Biosense 3 software and converted to the viscosity of the sample, v_s , using the given equation:

$$\Delta f_n = -\frac{n^{1/2} f_1^{3/2} (v_s \rho_s)^{1/2}}{(\pi \rho_q \mu_q)^{1/2}}$$
 [6]

where ρ_s is the density of the solution, ρ_q is the density of quartz (2.648 g/cm³), and μ_q is the Shear Modulus of quartz (2.947x10¹¹ gcm⁻¹s⁻²). f_I is the fundamental frequency of the crystal.

The concentrated ZnSO₄ electrolyte was further analyzed with FTIR and Raman spectroscopy. Diamond ATR-FTIR spectroscopy (ThermoFisher Nicolet iS50R) was used for the dilute solution (0.15mol/kg) and the most concentrated (0.25mol/kg). The same solutions were analyzed with Raman spectrometry (Horiba XploRA plus) for comparison of vibrational characteristics. *In situ optical triangular cell prototype:* An open-ended quartz triangular cuvette was sealed into

two custom caps and connected to the optical table stage in the path of the HeNe laser (Figure 1c).

The caps housed triangular zinc electrodes to close both ends of the diffusion column. This electrochemical cell was connected to a potentiostat (Metrohm Autolab PGSTAT302N) to test the response of the cell at a low current. The cell was positioned for the laser to pass across the surface of the zinc anode, and its response to a current pulse (0.5mA, 5s) was recorded by the detector.

Results and Discussion

Concentration-dependent beam deflection:

Shown in Figure 2a (green square points, right axis) are the concentration-dependent refractive index measurements for ZnSO₄ solutions from 0.10 mol/kg to 2.6 mol/kg, which increases from ca. 1.3380 to 1.3982. A nonlinear relationship is observed in a wide range of concentrations. The fitted green curve is found to follow the following function $n=1.33+0.0500m-0.0176m^2+0.00367m^3-0.000216m^4$ ($R^2=1$). It should be noted that the refractive index of electrolytes is typically considered to be linear in a small concentration range.¹³

A model was developed to test the relationship between beam deflection and the concentration of the electrolyte. Using Snell's law (Figure 1b) and the refractive index of the electrolyte as a function of concentration, the theoretical position of the deflected beam can be calculated. The intermediate angle of refraction, inside the cell θ_3 , is simply described by Snell's law:

$$n_1 \sin \theta_1 = n_3 \sin \theta_3 \tag{7}$$

Where n_1 and θ_1 are the refractive index of air and angle of incidence respectively, and n_3 is the concentration-dependent refractive index of electrolyte. Taking into consideration the $\pi/4$ geometry of the cell, we can calculate the changing final angle of refraction, θ_6 , of the beam as it leaves the cell:

$$\theta_6 = \arcsin\left(\left\{n_3 \sin\left(\frac{\pi}{4} - \theta_3\right)\right\} / n_1\right)$$
 [8]

Combining Equations 7 and 8 and inserting into a trigonometric calculation with the distance from the cell to the detector, d, we can determine the beam deflection across the detector, p:

$$p = -d* \tan \left[arc \sin \left(n_3 \sin \left\{ \frac{\pi}{4} - arc \sin \left(\frac{n_1 \sin \theta_1}{n_3} \right) \right\} / n_1 \right) \right]$$
 [9]

The model (Equation 9) was used to test the linear relationship between beam deflection and concentration of the electrolyte. The input function, n_3 , taken from experimental refractive index measurements, produced theoretical deflection vs. concentration data (Figure 2a, gray line, left axis). The relationship was shown to be linear over the range of concentrations from 0.10 mol/kg to 2.6 mol/kg. The fitted function (Figure 2a, red line) is p = -0.149m - 0.357 ($R^2 = 0.997$) when d is 400 mm. Note d is adjustable between 400 and 800 mm depending on the concentration of samples tested in the triangle column.

The experiment using the position sensing detector to monitor the beam deflection further proves the strong linear relationship between p and c, as shown in Figure 2b (red square points, left axis). The fitted red line follows the function p = 28.3c - 42.3 ($R^2 = 0.999$), demonstrating the concentration of the electrolyte can be tracked by the beam deflection. The linear calibration curve, built upon the experimental data of beam deflection vs. concentration, allowed the conversion of the laser beam position into concentration values during the diffusion tests. Each reported diffusion coefficient required a unique detector position, d, depending on the range of angles of refraction. The detector was positioned to make use of the full width of the sensor during the calibration, optimizing the sensitivity of the instrument. To increase the accuracy of the measurements, a calibration was run for each new detector position before and after the diffusion experiment to produce an average calibration curve. It is found a linear relationship holds true for all the electrolytes tested in the work. This allowed for simple processing of the position data from the detector to accurately produce a concentration profile.

The electrolyte concentrations were also converted from molality to molarity using a simple density calibration. An example of the molality and molarity calibration in the same range can be seen in Figure 2b (green line, right axis). The linear fitted function is c = 0.790m + 0.149 ($R^2 = 1$).

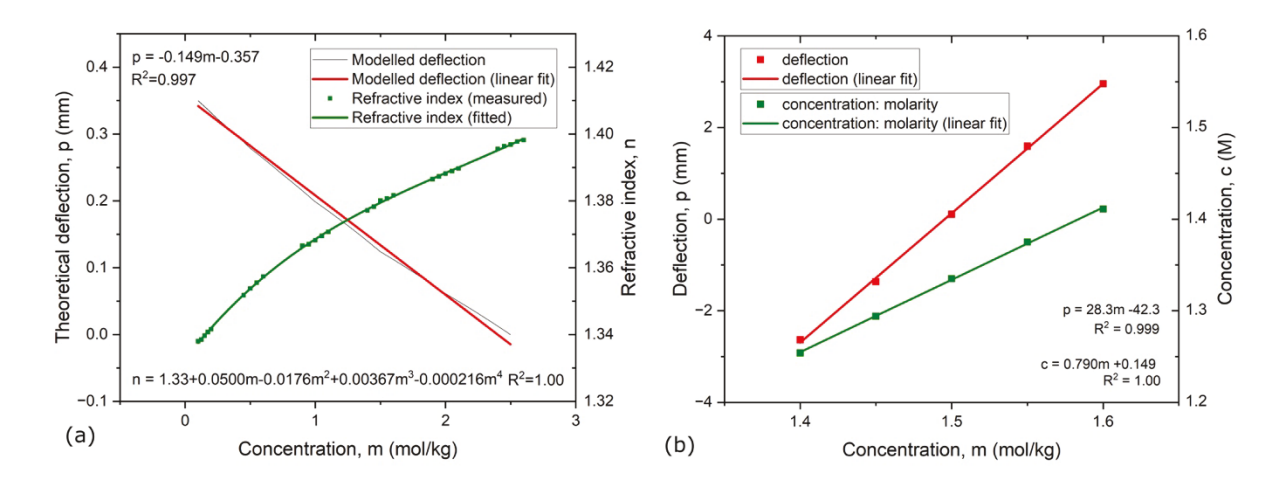


Figure 2. (a) concentration-dependent refractive index of ZnSO₄ electrolytes (green, right axis) and theoretical position of the laser beam with varying concentrations of ZnSO₄ electrolytes (gray, left axis) and its linear fit (red); (b) calibration curves to convert beam deflection position to the concentration of electrolyte (red, left axis) and molality to molarity (green, right axis).

Diffusion coefficient measurements: With two different concentrations of electrolyte layered inside the quartz cell, the restricted diffusion model is considered as the concentration gradient reaches the ends of the column. The resulting exponential shape of the time-dependent concentration profile qualitatively aligns with Harned and French's Fourier series (Equation 4), but over 48 hrs rapid convergence can be observed by Newman's linear relationship with $ln(c_{r}-c)$ and time. When the time-resolved $ln(c_{r}-c)$ reaches linearity, the slope of the linear region is extracted and the diffusion coefficient is calculated using Equation 5.

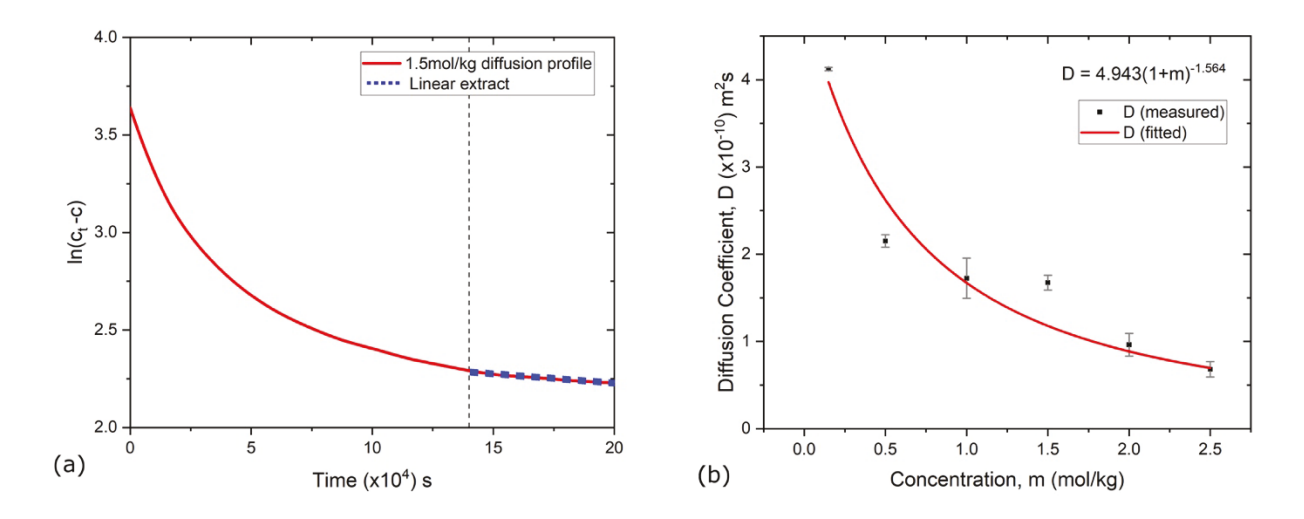


Figure 3: (a) Diffusion curve for 1.5 kg/mol ZnSO₄ electrolyte by mixing of electrolytes of 1.45 and 1.55 mol/kg; (b) diffusion coefficients for concentrations between 0.15 mol/kg and 2.5 mol/kg.

The acquired beam deflection data for each coupled solution, e.g. 1.45 and 1.55 mol/kg, was converted into the time-resolved concentration profile. A signature diffusion curve was successfully observed for each concentration couple using the method described, and an example of the time-resolved $ln(c_{I^*}c)$ curve (1.5 mol/kg) is shown in Figure 3a with the linear region highlighted in blue dashed line. The method was equally successful for dilute and concentrated solutions and the resulting diffusion coefficients are on the order 10^{-10} m²/s (Figure 3b, black square points), decreasing as samples become more concentrated. Concentration-dependent diffusion coefficients are fitted using the function $D = 4.943(1 + m)^{-1.564}$ (red curve). Diffusion coefficients measured in our experiment are slightly lower than the limited literature values. Our experiments ran at 22.4°C, slightly cooler than most reported values for ZnSO₄, therefore smaller diffusion coefficients should be expected. Also noted is many methods experience issues with inflated diffusion coefficients due to the convection of liquid samples. Overall, the optical method based on the refraction of the laser beam is successful in characterizing the diffusion coefficient of the concentrated battery electrolytes.

The method based on a refractive laser beam was simple to set up and shows potential for precise measurement due to the highly responsive nature of the solution and detector apparatus. By adjusting the distance between the detector and the triangle cuvette, the sensitivity of the experimental setup can be optimized. Maintaining a stable temperature throughout the experiment was key to successful measurements since diffusion and refractive index are a function of temperature. It was also important to keep a clear optical path for the laser, with the quartz cell remaining clear of fine crystals which tend to form if the cell is not sufficiently clean.

Physical properties and microstructures of ZnSO₄ electrolytes: Physiochemical properties and microstructures of battery electrolytes are correlated, e.g., electrolytes with high viscosity typically come with smaller diffusion coefficients and more ion pairs or aggregates.²⁷ With the diffusion coefficient measured using the novel optical method, we continued to characterize the same electrolyte and correlate the physical properties and microstructures, including viscosity, conductivity, infrared, and Raman spectroscopy.

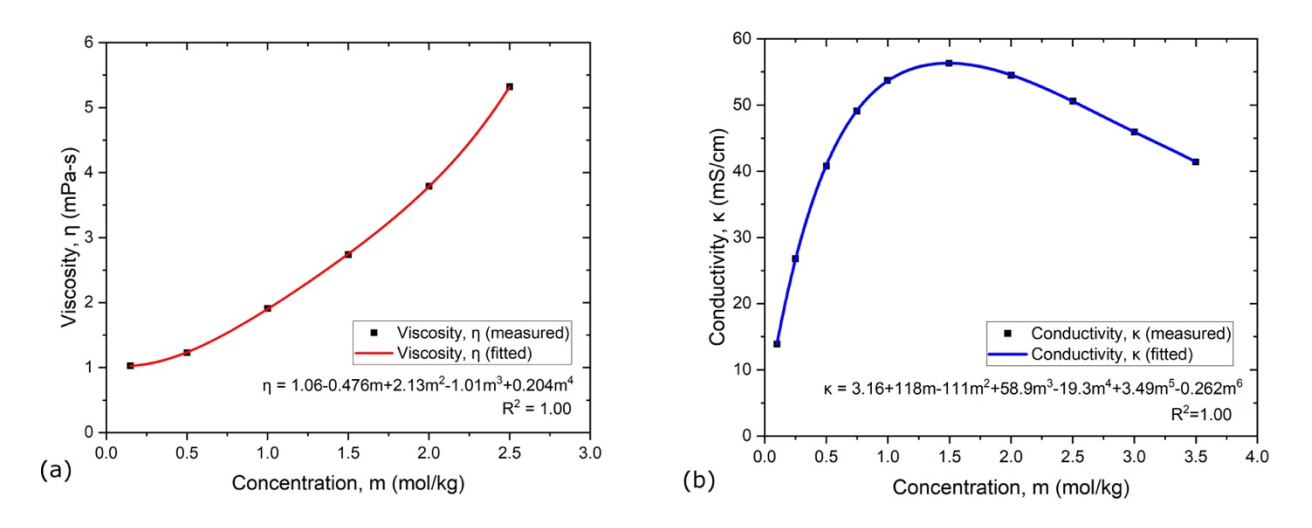


Figure 4. Concentration-dependent viscosity (a) and conductivity (b) of ZnSO₄ electrolytes.

The results obtained from the QCM-I experiment demonstrate a clear relationship between the concentration of ZnSO₄ and the viscosity of the electrolyte. As shown in Figure 4a, as the concentration of ZnSO₄ increases, the viscosity of the electrolyte also increases from 1 to 5.5 mPa-

s. The concentration-dependent viscosity is fitted using the function $\eta = 1.06 - 00.476m + 2.13m - 1.01m^3 + 0.204m^4$ ($R^2 = 1$). The increase in viscosity can be attributed to the increased interaction between ions, leading to stronger interionic forces and hindrance to ionic motion. Consequently, the higher concentration of ZnSO₄ results in a more viscous electrolyte.

The bivalency of zinc ions allows for high charge density and opportunity for efficient transportation of charge in electrolytes. As expected, the conductivity of ZnSO₄ was found to quickly increase with concentration, although by 1.0 mol/kg this relationship slowed, and the peak conductivity was found at 1.5 mol/kg (Figure 4b). Although more charge is present at higher concentrations, the charge density leads to stronger coulombic interactions, e.g., ion-ion repulsion and ion pairing. The resulting increase in Stokes's radius leads to a maximum in conductivity due to competition between increased ionic density and reduced mobility.²⁸ This behavior negatively impacts the diffusion coefficient, which is much smaller for more concentrated samples (Figure 3b). The concentration-dependent conductivity of ZnSO₄ solution is fitted using the polynomial function $\kappa = 3.16 + 118m - 111m^2 + 58.9m^3 - 19.3m^4 + 3.49m^5 - 0.262m^6$ ($R^2 = 1$) The relationship between conductivity, viscosity, temperature, and concentration is often described by Debye-Huckel-Onsager theory in dilute systems, but more complex models are still being developed to fully account for interactions in concentrated systems.²⁹

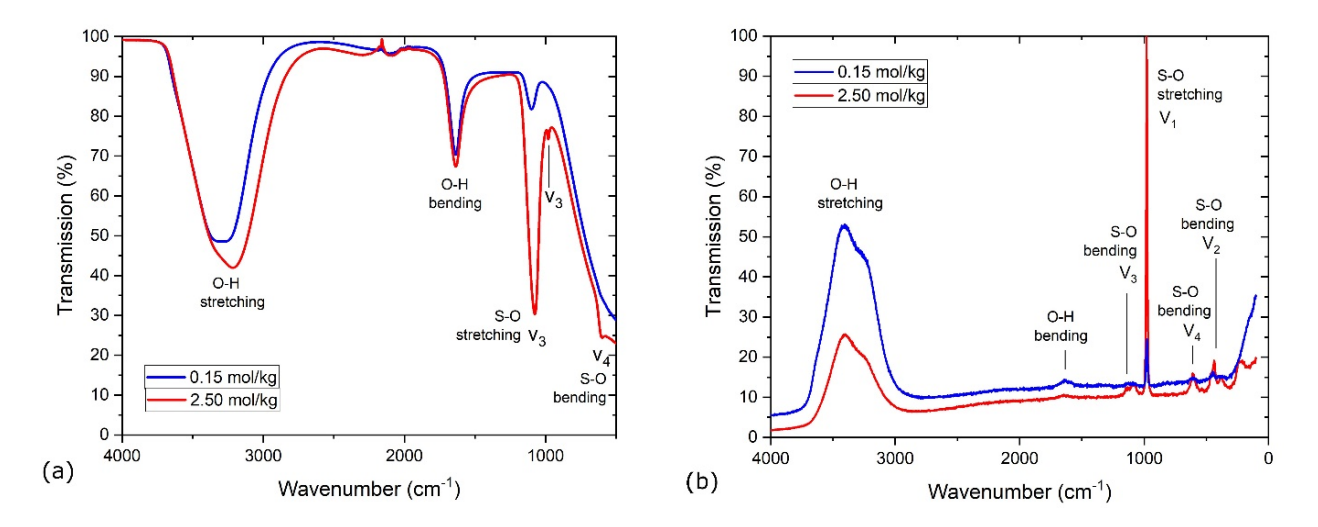


Figure 5. FTIR (a) and Raman (b) spectra for ZnSO₄ electrolytes of 0.15 ml/kg (blue) and 2.50 mol/kg (Red).

The charge density and polarization power of Zn^{2+} ions can be observed in the FTIR spectrum (Figure 5a). The OH stretching from the water in the dilute electrolyte can be seen at 3294 cm⁻¹. Despite the lesser ratio of water in the concentrated system, the stretching peak is more intense, broad, and shifted to a lower wavenumber, ca. $3216cm^{-1}$. This is due to increased ionic interactions, and the elongation and weakening of the O-H bond.³⁰ In more concentrated solutions, the increased presence of anions intensifies the IR signal from O-H stretching.³¹ The same effect can be seen on the scissor bending peak from the solvent around $1636cm^{-1}$. The asymmetry in the shape of the O-H stretching due to v_1 , v_3 stretching, and vibrational coupling in the hydrogen bond network is more prominent in the more concentrated solution for the FT-IR spectrum.³²

The sulfate anti-symmetric stretching peak at 0.15 mol/kg at 1100 cm⁻¹ (v₃ doubly and triply degenerate bending) is again redshifted for more concentrated systems (1075cm⁻¹) and is suggestive of the continued effect of polarity and interactions in the concentrated system. As expected, the intensity of the sulfate peak is larger for the concentrated solution due to its relative

abundance. With increased intensity and resolution, the v_3 non-degenerate and v_4 bending peaks of sulfate can also be observed at 980 cm⁻¹ and 600 cm⁻¹ respectively. ³³

Unlike IR spectroscopy, ions do not need to experience a change in dipole moment/charge density to be Raman active. This means the increased ionic interaction and shifting dipole in concentrated systems does not surge intensity in Raman spectral peaks as it does for IR peaks. The recorded Raman spectrums for 0.15 mol/kg and 2.5 mol/kg can be seen in Figure 4b for comparison. Water solvent can be observed by the weak peak at 1635 cm⁻¹ and the strong double peaks at 3250 cm⁻¹ and 3400 cm⁻¹. The inherent polarizability of ions is not affected by changes in concentration in the same way as dipole moment, and therefore as the concentration increases, the proportion of water decreases and O-H peaks become less intense.³⁴ The prominent sulfate peak can be seen at 980 cm⁻¹, which corresponds to the v₁ symmetric stretching vibrational mode. Only anti-symmetric stretching is IR active, and therefore this peak is not observed in the IR spectrum. The v₄ bending mode (which is identified by the large peak 1075cm⁻¹ in the IR spectra) can also be seen in the Raman spectra as a much weaker peak, more observable in the concentrated solution. The v₂ bending can also be seen at 435 cm⁻¹ on the Raman spectrum (this vibrational mode is also not IR active).³⁵

Overall, the IR spectrum (Figure 5a) helps describe the structural changes in the solution as it becomes more concentrated, which explains difficulties in maximizing its efficiency as an electrolyte. The Raman spectrum is a good comparison as it tells a more uniform story of increasing concentration, yet does not alone identify specific issues with dipole formation and bond weakening in concentrated solutions.

Future application of triangular optical cell: Following the success of the triangular optical cell for measurement of diffusion coefficients, it seemed like a natural evolution to develop an *in situ*

refractive beam using a similar cuvette, which could monitor the variation of the electrolyte in the working battery. Shown in Figure 6a is a prototype of the *in situ* optical triangular cell with two pieces of triangular zinc metal as electrodes sealing the ends of the cell.

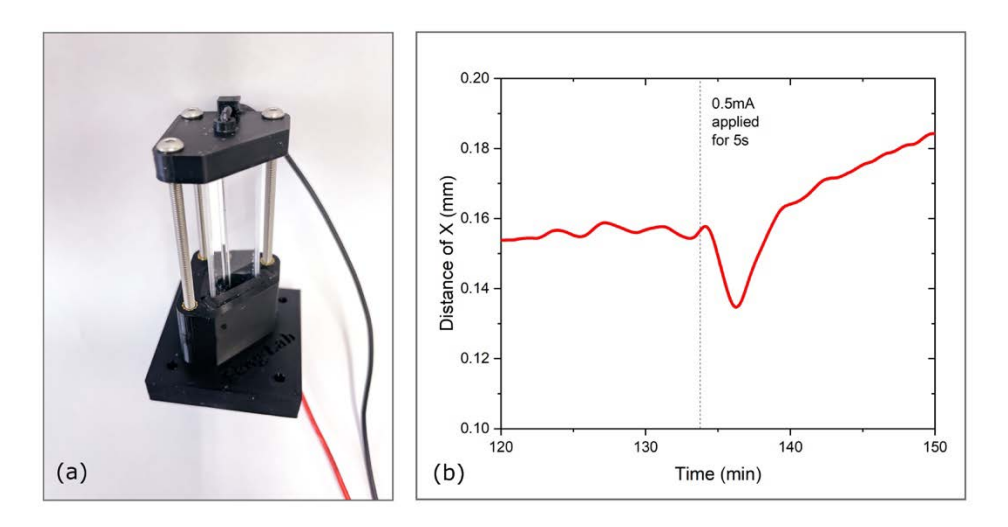


Figure 6. (a) Prototype of *in situ* optical triangular cell. (b) Optical response of cell to pulsed current (0.1 mA, 5 s) in 2.5mol/kg ZnSO₄ electrolyte.

When passing 0.5 mA current for 5s, the triangular optical cell successfully showed a sudden deflection in position followed by a slightly slower relaxation as shown in Figure 6b. As expected, this response is caused by the production of cell concentration gradient once current is applied. For the larger currents and longer run times, it was successful in displaying the general trend but led to considerable noise (data not shown), which may be caused by side reactions on the electrodes, e.g., the production of hydrogen gas. Further work in our lab is ongoing to achieve quantitative characterization of the electrolyte using *in situ* triangular cell, and it will be reported in due course.

Conclusion

In this work, a highly sensitive optical method using a refractive laser beam through triangular diffusion column was developed to measure the diffusion coefficient of concentrated battery

electrolytes. The novel method based on the Snell's law can be applied to all liquid phase electrolytes since the refractive index is concentration dependent for all liquid electrolytes. A strong linear relationship is found between the beam deflection and the concentration of electrolytes, which is utilized to characterize the concentration profile in the course of diffusion. Diffusion coefficients are calculated using a model based on OSM theory, accounting for multicomponent concentrated systems in a restricted diffusion column. The measured diffusion coefficients are between 4.12×10^{-10} m²/s for 0.15 mol/kg ZnSO₄ and 0.681×10^{-10} m²/s for 2.5 mol/kg ZnSO₄ at 22.4 °C. The profile of concentration-dependent diffusion coefficients follows a non-linear inverse relationship described by the function $D=4.943(1+m)^{-1.564}$.

We further characterize the conductivity, viscosity, as well as microstructure of ZnSO₄ electrolyte using FT-IR and Raman spectroscopy. High concentration electrolytes with more ion pairs show increased viscosity which ultimately leads to smaller diffusion coefficients. Interionic interactions also led to reduced conductivity at concentrations beyond 1.5mol/kg, despite the increased charge density of concentrated solutions. FT-IR spectrums allowed analyzation of increased charge density, which surged the intensity of the O-H stretching peak in concentrated electrolytes, despite the decrease in the ratio of water. Competition between charge density and viscosity continues to challenge the efficiency of concentrated electrolytes.

Lastly, we demonstrate the prototype *in sit*u triangular cell to characterize the electrolyte in working batteries. The cell responds to short, low-voltage pulses with beam deflection and relaxation, and offers an opportunity as a novel in situ spectroscopic tool to characterize the battery electrolyte.

Acknowledgments

The authors thank Kidus Yohannes and Michael Frailey (University of Nevada, Las Vegas) for their assistance in the lab. This work is supported by a grant from NSF (CBET-2243098).

References

- 1. K. Amine, R. Kanno, and Y. Tzeng, MRS Bull., 39, 395-401 (2014).
- 2. D. Larcher and J.-M. Tarascon, *Nat. Chem.*, **7**, 19–29 (2015).
- 3. https://iopscience.iop.org/article/10.1149/2.1221802jes.
- 4. M. Weiss et al., Adv. Energy Mater., 11, 2101126 (2021).
- 5. J. Newman and K. E. Thomas-Alyea, Wiley.com (2004)
- 6. S. G. Stewart and J. Newman, J. Electrochem. Soc.
- 7. A. M. Bizeray, D. A. Howey, and C. W. Monroe, J. Electrochem. Soc., 163, E223 (2016).
- 8. E. O. Stejskal and J. E. Tanner, J. Chem. Phys., 42, 288–292 (2004).
- 9. L. Deng et al., Chin. Chem. Lett., 28, 362–366 (2017).
- 10. R. Takekawa and J. Kawamura, J. Magn. Reson., **326**, 106958 (2021).
- 11. K. Timachova, J. Newman, and N. P. Balsara, J. Electrochem. Soc., 166, A264 (2019).
- 12. J. Hrabe, G. Kaur, and D. N. Guilfoyle, *J. Med. Phys. Assoc. Med. Phys. India*, **32**, 34–42 (2007).
- 13. J. Newman and T. W. Chapman, AIChE J., 19, 343–348 (1973).
- 14. F. Liu, G. Kolesov, and B. A. Parkinson, J. Electrochem. Soc., 161, H3015 (2014).
- 15. J. R. Hazel and B. D. Sidell, *Anal. Biochem.*, **166**, 335–341 (1987).
- 16. R. L. Kay and C. A. Kraus, *J. Am. Chem. Soc.*, **81**, 2270–2270 (1959).
- 17. H. J. V. Tyrrell and K. R. Harris, in *Diffusion in Liquids*, H. J. V. Tyrrell and K. R. Harris, Editors, p. 104–257, Butterworth-Heinemann (1984)
- 18. K. Nishikawa, Y. Fukunaka, T. Sakka, Y. H. Ogata, and Selman, *J. Electrochem. Soc.*, **153**, A830–A834 (2006).
- 19. L. Wei et al., Opt. Lasers Eng., 126, 105867 (2020).
- 20. B. Chen, J. Xuan, G. J. Offer, and H. Wang, Appl. Energy, 279, 115687 (2020).
- 21. J. Fawdon, J. Ihli, F. L. Mantia, and M. Pasta, Nat. Commun., 12, 4053 (2021).
- 22. L. Onsager, Ann. N. Y. Acad. Sci., 46, 241–265 (1945).

- 23. J. Newman, D. Bennion, and C. W. Tobias, *Berichte Bunsenges. Für Phys. Chem.*, **69**, 608–612 (1965).
- 24. S. Umino and J. Newman, J. Electrochem. Soc., 144, 1302–1307 (1997).
- 25. J. G. Albright and D. G. Miller, J. Solut. Chem., 4, 809–816 (1975).
- 26. Y. Awakura, T. Doi, and H. Majima, *Metall. Trans. B*, **19**, 5–12 (1988).
- 27. I. Avramov, J. Non-Cryst. Solids, 355, 745-747 (2009).
- 28. J. Barthel, H. J. Gores, and G. Schmeer, *Berichte Bunsenges. Für Phys. Chem.*, **83**, 911–920 (1979).
- 29. Y. Avni, R. M. Adar, D. Andelman, and H. Orland, *Phys. Rev. Lett.*, **128**, 098002 (2022).
- 30. J. Joseph and E. D. Jemmis, J. Am. Chem. Soc., 129, 4620–4632 (2007).
- 31. N. Kitadai et al., *J. Solut. Chem.*, **43**, 1055–1077 (2014).
- 32. T. Seki et al., J. Phys. Chem. Lett., 11, 8459-8469 (2020).
- 33. M. D. Lane, Am. Mineral., 92, 1–18 (2007).
- 34. W. W. Rudolph, M. H. Brooker, and P. R. Tremaine, J. Solut. Chem., 28, 621-630 (1999).
- 35. W. W. Rudolph, M. H. Brooker, and P. Tremaine, Z. Für Phys. Chem., 209, 181–207 (1999).